Optimal Surface Deployment Problem in Wireless Sensor Networks

Miao Jin[1], Guodong Rong[2], Hongyi Wu[1], Liang Shuai[3], and Xiaohu Guo[3]
[1]The Center for Advanced Computer Studies, University of Louisiana at Lafayette. {mjin,wu}@cacs.louisiana.edu
[2]NVIDIA Corporation, Santa Clara, CA. {rongguodong}@hotmail.com
[3]Department of Computer Science, University of Texas at Dallas. {shuai,xguo}@utdallas.edu

***Abstract*—Sensor deployment is a fundamental issue in a wireless sensor network, which often dictates the overall network performance. Previous studies on sensor deployment mainly focused on sensor networks on 2D plane or in 3D volume. In this paper, we tackle the problem of optimal sensor deployment on $3D$ surfaces, aiming to achieve the highest overall sensing quality. In general, the reading of a sensor node exhibits unreliability, which often depends on the distance between the sensor and the target to be sensed, as observed in a wide range of applications. Therefore, with a given set of sensors, a sensor network offers different accuracy in data acquisition when the sensors are deployed in different ways in the Field of Interest (FoI). We formulate this optimal surface deployment problem in terms of sensing quality by introducing a general function to measure the unreliability of monitored data in the entire sensor network. We present its optimal solution and propose a series of algorithms for practical implementation. Extensive simulations are conducted on various 3D mountain surface models to demonstrate the effectiveness of the proposed algorithms.**

I. Introduction

The emerging wireless sensor networks have been envisioned for a diversity of autonomous monitoring and actuation applications on 2D plane, 3D surface and 3D volume. With its substantial impact on network performance, sensor deployment has been a central problem in wireless sensor network research. Previous work on sensor deployment mainly focused on networks with their Field of Interest (FoI) on 2D plane [1]–[20] or in 3D volume [21]–[26]. However, recent study [27] reveals that sensor deployment on 3D surface is fundamentally different from its counterpart on 2D plane or in 3D volume, exhibiting surprising challenges with provable NP complete property to determine optimal solution with full coverage. Thus, early developed deployment strategies for 2D planar or 3D volumetric networks cannot be applied on 3D surface networks directly.

In this research, we consider a FoI on a 3D surface, and tackle the problem of optimal sensor deployment for maximized overall sensing quality. In general, a sensor node does not always make perfect measurement. Instead, its reading exhibits inevitable error, which often depends on the distance between the sensor and the target being sensed, as observed in a wide range of applications, e.g., for monitoring pollution, radiation, acoustics, and vibration. With a given set of sensors, a sensor network offers different accuracy in data acquisition when they are deployed in different ways in the FoI.

There are a handful of works that address the sensing quality of sensor deployment, which are all based on 2D sensor networks with different viewpoints for problem formulation. Multiple coverage, where each point is covered by at least k different sensors, is proposed to improve the monitoring quality in [28]–[32]. Event probability density is considered in [33]–[35] to guide mobile sensors to concentrate in areas with high event density and maintain full coverage at the same time. A local control law is proposed in [36] where each agent takes the value of sensory function which indicates the relative importance of different areas in the FoI and the sensing unreliability of the sensor measurement into a cost function to make moving decision.

In this paper, we consider a given set of sensors deployed on general 3D surfaces with possible concave boundary condition. We assume that the sensors can be deployed at any pre-determined locations. We formulate the optimal surface deployment problem by introducing a general function to measure the unreliability of sensor data, aiming to maximize the overall sensing quality of the entire sensor network. We show that the optimal deployment can be achieved under a generalized centroidal Voronoi partition. With the insights gained from conformal parametrization, we propose a series of practical algorithms to realize sensor deployment on general 3D surfaces that minimizes the network-wide unreliability of sensor data. The main results and contributions of this work are summarized as follows:

- We introduce a new model to formulate the problem of sensor deployment on 3D surface.
- We present the optimal solution for 3D surface sensor deployment with minimized overall unreliability.
- A series of algorithms are proposed to approximate the optimal solution, with extensive simulations conducted to verify their effectiveness.

The rest of the paper is organized as follows: Sec. II formulates the optimal surface deployment problem. Sec. III shows its optimal solution. Sec. IV presents the theoretical insights of our proposed algorithms. Sec. VI elaborates the algorithmic details, followed by simulation results in Sec. VII. Sec. IX concludes the paper and discusses our future work.

II. Problem Formulation

Before giving the formal definition of the optimal surface deployment problem studied in this paper, we first introduce the surface model and the wireless sensor network model employed in this research.

A. Surface Models

It is rare in reality the deployment surface is either closed or with handles, so in our study we focus on surface models with disk topology (i.e., open surface with single boundary). Surfaces can have complicated geometric shapes and complex boundary conditions including concave case as shown in Sec. VII. They do not need to be single valued surfaces as required in [27] (i.e., any two points of the surface should have two different projections on the x-y plane), and are not subject to any restriction on their height.

B. Models of Wireless Sensor Network

We assume stationary and homogeneous sensors deployed on surfaces. They do not move after deployment and have the same sensing radius and identical sensing capacity. The accuracy of their collected data depends on the distance between the sensor and the target point to be sensed.

C. Optimal Surface Deployment Problem

As discussed in Sec. I, sensors do not always make perfect measurement, but exhibit unreliability that in general depends on the distance between the sensor and the target to be sensed. We define the following function to measure such unreliability for data collected from a single point.

Definition 1: Let p_i denote the position of Sensor i on a FoI denoted as A. Given a point q on A, the *sensing unreliability function* $g(||q-p_i||)$ describes how unreliable the measurement of the information at Point q sensed by Sensor i at p_i is, where $||\cdot||$ represents the distance between q and p_i.

The specific form of $g(||q-p_i||)$ is application-dependent. We consider $g(||q-p_i||)$ as a general function in this research, as long as it is continuous and strictly increasing. Note that $g(||q-p_i||)$ will go to infinity if the distance is long enough.

Definition 2: Given a set of n sensors deployed on A, let $P=\{p_i|1\le i\le n\}$ be the set of positions of all sensor nodes. A sensing partition of A is defined as $\mathbb{V}=\{\mathbb{V}_i|1\le i\le n\}$ where $\mathbb{V}_i$ represents the sensing region of a sensor at position p_i. Note that the union of $\mathbb{V}_i$ covers the whole A. A point of A may be within sensing ranges of several sensor nodes, but belongs to only one sensing region of a sensor.

The following equation gives the sensing unreliability of a single sensor.

Definition 3: Given Sensor i, the sensing unreliability of data collected over its sensing Region $\mathbb{V}_i$ on A is defined as:

$$G_i(p_i,\mathbb{V}_i)=\int_{q\in\mathbb{V}_i} g(||q-p_i||)dq, \tag{1}$$

where q is a point inside $\mathbb{V}_i$.

Summing over all sensors, we arrive at the overall sensing unreliability of the entire network, given by the following definition.

Definition 4: Given a set of n sensors deployed on A, the overall sensing unreliability of data collected by the entire network is defined as:

$$G(P,\mathbb{V})=\sum_{i=1}^{n}\int_{q\in\mathbb{V}_i} g(||q-p_i||)dq. \tag{2}$$

With the above definitions, we can formulate the optimal surface deployment problem (OSDP) as follows.

Definition 5: Given a set of n sensors to be deployed with FoI on a 3D surface, the *optimal surface deployment problem* (OSDP) is to identify P and $\mathbb{V}$ such that $G(P,\mathbb{V})$ is minimized.

III. Optimal Solution

To find the optimal solution of OSDP, we start our study from a simplified version of this problem, which is defined as:

Definition 6: Given a set of n sensors deployed on a field of interest A, the *optimal surface sensing problem* (OSSP) is to identify $\mathbb{V}$ with fixed P such that $G(P,\mathbb{V})$ is minimized.

With given A and fixed P, there are different ways to assign the sensing region to each sensor which induces infinitely possible solutions for the OSSP. We prove that the Voronoi partition based sensing regions achieve the optimal solution of the surface sensing problem.

Let's first give the definition of the Voronoi partition.

Definition 7: A *Voronoi partition* is a partition of the space according to the distances to a discrete set of objects (i.e., sensors in our setting), $P=\{p_i|1\le i\le n\}$, called sites in the space. A Voronoi cell, or a Voronoi region, $\mathbb{V}_i$, of a site p_i is the region of points that are closer to p_i than to any other sites, that is

$$\mathbb{V}_i=\{q\in A \mid ||q-p_i||\le||q-p_j||,\forall j\ne i\}. \tag{3}$$

We let $\mathbb{V}(P,A)$ denote the Voronoi partition generated by P on A.

The following Lemma proves that $\mathbb{V}(P,A)$ minimizes the total unreliability of data collected from the sensor network.

Lemma 1: For a fixed placement of sensors (i.e., $P=\{p_i|1\le i\le n\}$) on A, the Voronoi partition $\mathbb{V}(P,A)$ minimizes the unreliability function $G(P,\mathbb{V})$.

Proof: Suppose we have a partition $\Omega=(\Omega_1,\Omega_2,\ldots,\Omega_n)$ which is different from Voronoi partition $\mathbb{V}=(\mathbb{V}_1,\mathbb{V}_2,\ldots,\mathbb{V}_n)$. Let's consider an arbitrary point q that is in Cell $\mathbb{V}_i$ in the Voronoi partition and at the same time belongs to Ω_j under the other given partition. Because of the definition of the Voronoi partition, we always have

$$||q-p_i||\le||q-p_j||.$$

Note the function g to measure the unreliability is a strictly increasing function. So,

$$g(||q-p_i||)\le g(||q-p_j||).$$

Since Ω is not a Voronoi partition, the above formula must hold with strict inequality on those regions which are not exactly the same as the Voronoi regions. Thus,

$$G(P,\mathbb{V})<G(P,\Omega),$$

so that $G(P,\mathbb{V})$ is minimized when the sensing region is the Voronoi partition of the sites. ■

Lemma 1 shows that the Voronoi partition is optimal under the assumption of fixed sensor placement (i.e., $P = \{p_i | 1 \leq i \leq n\}$). However, given a set of n sensors, there are infinite ways to place them on A, with each inducing a different Voronoi partition. It is clearly impossible to check all of them in order to identify which one achieves the minimal $G(P,\mathbb{V})$. Theoretical understanding is needed to discover the optimal P, whose induced Voronoi partition minimizes $G(P,\mathbb{V})$.

To this end, we introduce the concept of centroidal Voronoi partition, which was first given by Du et al. [37], although similar concepts have been studied in different areas before. The centroidal Voronoi partition has a wide usage in different application areas. The readers are referred to [36]–[41] for extended discussions.

Definition 8: The *mass centroid*, $\widetilde{p_i}$, of the Voronoi region $\mathbb{V}_i$ is defined as:

$$\widetilde{p_i} = \frac{\int_{q\in\mathbb{V}_i} q\rho(q)dq}{\int_{q\in\mathbb{V}_i} \rho(q)dq}, \tag{4}$$

where $\rho(q)$ is the density function defined in A and $\rho(q) \geq 0$.

Definition 9: Given $P = \{p_i | 1 \leq i \leq n\}$. If the mass centroid $\widetilde{p_i}$ satisfies $\widetilde{p_i} = p_i$ for every $\mathbb{V}_i$ $(1 \leq i \leq n)$, then $\mathbb{V} = \{\mathbb{V}_i | 1 \leq i \leq n\}$ is a *centroidal Voronoi partition*.

In other words, a centroidal Voronoi partition is a Voronoi partition such that each site is located at the mass centroid of its corresponding Voronoi region with respect to a given density function. For any given set of sites, a centroidal Voronoi partition always exists, although not necessarily unique [37].

Now we show that given a set of sensors, the placement under a generalized centroidal Voronoi partition is optimal (i.e., with minimum $G(P,\mathbb{V})$). More specifically, we have the following theorem.

Theorem 1: For a given set of n sensors on A, the optimal sensor placement $P = \{p_i | 1 \leq i \leq n\}$ and corresponding partition $\mathbb{V} = \{\mathbb{V}_i | 1 \leq i \leq n\}$ that together minimize the unreliability function $G(P,\mathbb{V})$ are achieved when $\mathbb{V}$ is the Voronoi partition of P and p_i is the generalized centroid of $\mathbb{V}_i$, $\forall i$, $1 \leq i \leq n$.

Proof: Let us examine the first variation of G with respect to a single sensor placement. Suppose that all other sensors remain at their original positions and only the ith sensor slightly changes its location from p_i to $p_i + \varepsilon p_i$ ($||\varepsilon p_i|| \approx 0$). Let $\mathbb{V}$ and $\overline{\mathbb{V}}$ be the Voronoi partitions generated by $(p_1,\ldots,p_i,\ldots,p_n)$ and $(p_1,\ldots,p_i+\varepsilon p_i,\ldots,p_n)$, and $\mathbb{V}_i$ and $\overline{\mathbb{V}}_i$ be the Voronoi regions of the ith sensor in $\mathbb{V}$ and $\overline{\mathbb{V}}$, respectively. N_i be the set of indices of the Voronoi regions adjacent to $\mathbb{V}_i$. With respect to the slight move εp_i, the Voronoi partition slightly changes, but this change occurs only in $\mathbb{V}_i$ and its adjacent Voronoi regions, i.e. $\mathbb{V}_j, j \in N_i$. Their neighboring relations remain the same. So we have:

$$\begin{aligned} &G((p_1,\cdots,p_i+\varepsilon p_i,\cdots,p_n),\overline{\mathbb{V}}) - G((p_1,\cdots,p_i,\cdots,p_n),\mathbb{V}) \\ &= \int_{\overline{\mathbb{V}}_i} g(||q-p_i-\varepsilon p_i||)dq - \int_{\mathbb{V}_i} g(||q-p_i||)dq \\ &+ \sum_{j\in N_i} [\int_{\overline{\mathbb{V}}_j} g(||q-p_j||)dq - \int_{\mathbb{V}_j} g(||q-p_j||)dq] \end{aligned}$$

By taking the limit $\varepsilon p_i \to 0$, we arrive at

$$\frac{\partial G}{\partial p_i} = -M_{\mathbb{V}_i}(C_{\mathbb{V}_i} - p_i), \tag{5}$$

where

$$M_{\mathbb{V}_i} = \int_{q\in\mathbb{V}_i} \frac{1}{||q-p_i||} \frac{dg(||q-p_i||)}{d||q-p_i||} dq, \tag{6}$$

and

$$C_{\mathbb{V}_i} = \frac{1}{M_{\mathbb{V}_i}} \int_{q\in\mathbb{V}_i} \frac{q}{||q-p_i||} \frac{dg(||q-p_i||)}{d||q-p_i||} dq. \tag{7}$$

We refer readers to [38] (pp. 543-546) for details of a similar derivation to get Equation 5. $C_{\mathbb{V}_i}$ is called the *generalized centroid*. G achieves local minimal when $p_i = C_{\mathbb{V}_i}$. Also as indicated in [38], such derivative result holds not only for $\mathbb{R}^2$, but also for $\mathbb{R}^n$. ■

Theorem 1 reveals that the generalized centroidal Voronoi partition results in an sensor deployment, which minimizes the unreliability function given in Definition 4. There exist efficient algorithms to compute a planar centroidal Voronoi partition [42], [43] and it is not difficult to convert them to compute the generalized centroidal Voronoi partition on plane with the pre-determined unreliability function. But algorithms designed on 2D plane do not directly provide a workable solution on 3D surfaces, especially when the surface has a complicated shape. On the other hand, the convex boundary constraint applies to the planar centroidal Voronoi partition algorithms available in the literature. Such strong constraints are clearly unpractical, given the FoI on surface is complex with possible concave boundary condition. We need to develop an approximation algorithm to efficiently extend the centroidal Voronoi partition on a planar convex shape to 3D surfaces.

IV. Approximate Solution from 2D to 3D

Surface parametrization can be viewed as a one-to-one mapping from a 3D surface to a planar domain. The most simple example of surface parametrization is the projection of a single valued surface expressed as $z = f(x,y)$ to plane, by removing z coordinates. We refer readers to [44]–[46] for thorough surveys on surface parametrization. Parameterizing 3D surfaces to plane provides a possible solution to extend the planar centroidal Voronoi partition to 3D surfaces by projecting computed 2D results back to 3D surfaces based on the inverse of the surface mapping. However we need a special surface parametrization method which can map general 3D surfaces to convex shape in plane without restrictions on the shape or the boundary conditions of the surfaces.

One surface parametrization method is conformal mapping, which is a bicontinuous function, $f : S \to \mathbb{C}$ from surface S to plane $\mathbb{C}$. According to the Riemann mapping theorem [47], a topological disk surface can be conformally parameterized to a unit disk on plane. One way to compute the conformal mapping from a surface to a planar unit disk is to use discrete surface Ricci flow. We will give a brief introduction of discrete surface Ricci flow in Section V. As a result, the

set of originally randomly deployed sensors on the surface is mapped to the planar disk by f accordingly. With the circular boundary condition, we can apply available algorithms [42], [43] to efficiently compute a centroidal Voronoi partition of the given set of sensors on the planar disk, then project them back to the surface based on f^{-1}. However, simply computing a centroidal Voronoi partition on mapped planar disk does not induce a centroidal Voronoi partition on surface. The reason is straightforward. The definition of the centroidal Voronoi partition is distance-based. For surfaces embedded in $\mathbb{R}^3$, except very few cases like cylinder, there exists no any surface parametrization method which preserves metric (distance) of surfaces from $\mathbb{R}^3$ to $2D$ plane, regardless of the mapped shape on the $2D$ plane [48].

So it is obvious that we can't simply adopt conformal parametrization method to achieve the approximation from 2D to 3D. We need to compensate the distance distortion when computing the generalized centroidal Voronoi partition on mapped planar disk. One appealing property of conformal mapping is that it preserves the surface Riemannian metric (distance) up to a scaling factor called conformal factor. The conformal factor cf at a point p on the surface can be computed as the ratio between the infinitesimal areas around p in the $3D$ surface and $2D$ mapped plane, i.e. $cf(p) = \frac{Area_{3D}(p)}{Area_{2D}(p)}$. Intuitively speaking, zooming in locally a conformal mapping, the mapping result on plane has no local distortion compared with the original surface embedded in $\mathbb{R}^3$, except compressed by cf. Thus, when computing the centroidal Voronoi partition on the mapped planar disk, we need to scale the compressed metric on disk back by some value related with cf. Denote the metric of the surface at point p as $d_{3D}(p)$, and the metric of the mapped planar disk at point p as $d_{2D}(p)$, they differ by

$$d_{3D}(p) = cf(p)^2 d_{2D}(p).$$

We refer readers to our previous work [49] for the details of the equation.

V. Discrete Surface Ricci Flow

Ricci flow was first introduced by Richard Hamilton for Riemannian manifolds of any dimension in his seminal work [50]. Later Chow and Luo proved a general existence and convergence theorem for the discrete Ricci flow on surfaces in [51].

To briefly introduce the concept of discrete surface Ricci flow, we start from the definitions of circle packing metric and discrete Gaussian curvature. Let $M = (V,E,F)$ denote a triangulated surface embedded in $\mathbb{R}^3$, consisting of vertices (V), edges (E), and triangle faces (F). Each vertex $v_i \in V$ is assigned a circle with radius γ_i. The radius function is denoted as $\Gamma : V \to \mathbb{R}^+$. The two circles at v_i and v_j of edge $e_{ij} \in E$ intersect with an acute angle ϕ_{ij}, which is called the *weight* of e_{ij}. The weight function is denoted as $\Phi : E \to [0, \frac{\pi}{2}]$.

The length of e_{ij} can be computed from γ_i, γ_j and ϕ_{ij} by the following cosine law:

$$l_{e_{ij}}{}^2 = \gamma_i{}^2 + \gamma_j{}^2 + 2\gamma_i\gamma_j \cos\phi_{ij}. \tag{8}$$

Definition 10 (Circle Packing Metric): (Thurston 1976 [52]) A circle packing metric of M includes Γ and Φ.

Discrete Gaussian curvature measures how curved the discrete surface is embedded in $\mathbb{R}^3$. It is defined as the angle deficit.

Definition 11 (Discrete Gaussian Curvature): The discrete Gaussian curvature K_i on a vertex v_i is defined as:

$$K_i = \begin{cases} 2\pi - \sum_{f_i^{jk} \in F} \theta_i^{jk}, & v_i \notin \partial M, \\ \pi - \sum_{f_i^{jk} \in F} \theta_i^{jk}, & v_i \in \partial M, \end{cases} \tag{9}$$

where θ_i^{jk} represents the corner angle attached to v_i in face $f_i^{jk} \in F$, and ∂M is the boundary of M.

Suppose M has an initial circle packing metric (Γ_0, Φ). Let u_i be the logarithm of γ_i associated with v_i. The discrete surface Ricci flow is defined as follows:

$$\frac{du_i(t)}{dt} = (\overline{K}_i - K_i), \tag{10}$$

where $\overline{K}_i$ and K_i are the target and current Gaussian curvatures at v_i, and t is the time. Discrete surface Ricci flow continuously deforms the circle packing metric according to the difference between the current and target Gaussian curvatures. Convergence of discrete surface Ricci flow is proved in [51]. The final circle packing metric induces the edge length which satisfies the target Gaussian curvature.

By setting the target Gaussian curvatures of vertices satisfying the circular boundary condition, i.e., $\overline{K_i} = 0$ for $v_i \notin \partial M$, and $\sum \overline{K_i} = 2\pi$ for $v_i \in \partial M$, the discrete surface Ricci flow deforms the circle packing metric of a topological disk surface. The induced edge lengths when the discrete surface Ricci flow converges embed the surface to a planar disk.

VI. Algorithms

There are many resources providing real 3D surface datas. The Shuttle Radar Topography Mission (SRTM) C-band data [53] is the most complete and high-resolution digital topographic database. Another data resource is Light Detection And Ranging data (LIDAR) [54]. They are elevation data with high accuracy and dense coverage. Points in these data sets are on a grid structure, so it is straightforward to convert them to a triangular surface structure. Based on the overall idea discussed in previous sections, we devise a series of triangular structure-based algorithms to solve the OSDP.

Fig. 1 illustrates the major steps of the algorithms. The algorithms start with an initially random deployment of a given set of sensors marked with red on a mountain surface approximated by $5k$ triangles, denoted as M, as shown in Fig. 1(a). The computed conformal mapping of the surface to a unit planar disk, denoted as $f : M \to D$, is shown in Fig. 1 (b) with the set of sensors mapped to the disk accordingly. Fig. 1(c) uses color encoding to illustrate the conformal factor cf, which measures the metric distortion of M on D. The computed generalized centroidal Voronoi partition on D based on its compensated metric is shown in Fig. 1 (d) with red points and marked polygons representing the computed sensor positions and their

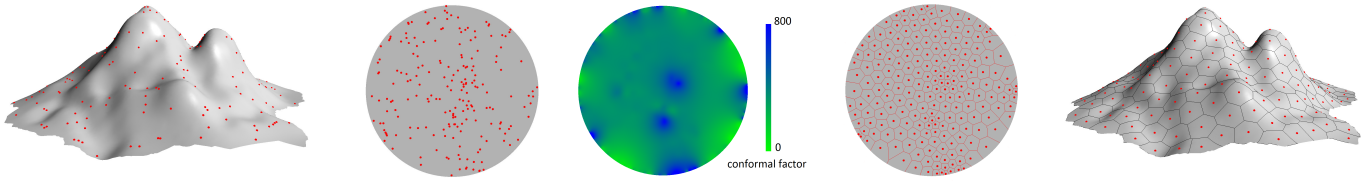

(a) (b) (c) (d) (e)

Fig. 1. Algorithms: (a) A set of sensors marked with red is randomly deployed on a mountain surface approximated by 5k triangles. (b) The mountain surface is mapped to a planar unit disk based on a conformal parametrization denoted as f, with sensors mapped to the disk accordingly. (c) Metric distortion of the surface on the disk is measured by conformal factor cf with color coded. (d) A generalized centroidal Voronoi partition of the set of sensors is computed on the planar disk based on its compensated metric, where points and polygons representing the computed sensor positions and their sensing regions respectively. (e) The set of sensors and their corresponding sensing regions are projected back to the surface based on f^{-1}.

sensing regions respectively. Fig. 1 (e) depicts the optimal deployment of the set of sensors and their sensing regions on M by projecting the computed generalized centroidal Voronoi partition on D to M based on f^{-1}. Note that in this example we choose the sensing unreliability increased quadratically along the distance with $g(||q-p_i||) = \frac{1}{2}||q-p_i||^2$. Next we elaborate each step of the proposed algorithms sequentially.

A. Parameterizing Surface to Disk

We parameterize a triangulated surface $M = (V,E,F)$ in $\mathbb{R}^3$ to a unit disk D in $\mathbb{R}^2$ using discrete surface Ricci flow as defined in Equation 10. The key idea of the algorithm is to set the target Gaussian curvature $\overline{k_i}$ of vertex $v_i \in V$ satisfying the circular boundary condition. The mapping result stored at each v_i is a complex number, called its uv value, which serves as the planar coordinates of v_i.

1) Preprocessing of boundary vertices: A boundary edge can be easily identified since it involves one face only. Let n denote the number of boundary edges of M.
2) Initialization: For each v_i, $u_i = 0$. If $v_i \in \partial M$, $\overline{k_i} = \frac{2\pi}{n}$, otherwise $\overline{k_i} = 0$.
3) The length of edge e_{ij} is computed as $l_{ij} = e^{u_i} + e^{u_j}$.
4) The corner angle θ_i^{jk} attached to v_i in face f_{ijk} is computed as $\theta_i^{jk} = cos^{-1}\frac{l_{ij}^2+l_{ki}^2-l_{jk}^2}{2l_{ij}l_{ki}}$.
5) Current discrete Gaussian curvature k_i of v_i is computed as Equation 9.
6) If all $|\overline{k_i}-k_i| < \varepsilon$, where ε is the threshold of the curvature error, the algorithm directly goes to the next step; otherwise, $u_i = u_i + \delta(\overline{k_i}-k_i)$, where δ is a small constant that indicates the step length. Then, the algorithm goes back to Step 3).
7) Planar embedding: The edge lengths (i.e., $\{l_{ij}|e_{ij} \in E\}$) are determined when the discrete surface Ricci flow converges. They will induce a planar disk embedding. Starting from any random f_{ijk}, set their uv values as: $uv(v_i) = (0,0)$, $uv(v_j) = (l_{ij},0)$, and $uv(v_k) = (l_{ki}cos\theta_i^{jk}, l_{ki}cos\theta_i^{jk})$. In a breadth first search way, for f_{jil} with exactly two vertices (e.g., v_i and v_j) having uv values, compute the uv value of v_l as the intersection point of the two circles centered at $uv(v_i)$ and $uv(v_j)$ with radii l_{il} and l_{jl}, respectively, and satisfying $(uv(v_l) - uv(v_i)) \times (uv(v_j) - uv(v_l)) > 0$. Repeat the above process until every vertex has its uv value.

B. Computing Generalized Centroidal Voronoi Partition

The Lloyd algorithm in [42] is one of the most popular iterative schemes for computing the centroidal Voronoi partition. Its convergence is proved in [43]. The Lloyd algorithm can be summarized by a three-step process:

1) Build the Voronoi partition of a set of sensors deployed inside a convex shape on plane.
2) Compute the centroid of each planar Voronoi region, and move each sensor onto its respective centroid.
3) Repeat Steps 1) and 2) until the moving distance of every sensor in Step 2) is smaller than a threshold.

Following the three basic steps, we first compute the Voronoi partition on the unit planar disk. There are multiple matured algorithms to compute the Voronoi partition of a set of discrete objects on a planar domain [55]. Our implementation employs the 2D Voronoi Diagram Adaptor of the CGAL library [56], one of the most popular computational geometry libraries.

Then we uniformly sample the unit disk using a a regular grid and perform the summation over all sampled points to approximate the integration in Equation 7:

$$M_{\mathbb{V}_i} = \sum_{q \in \mathbb{V}_i} cf(q)^2 \frac{1}{||q-p_i||} \frac{dg(||q-p_i||)}{d||q-p_i||}, \tag{11}$$

and

$$C_{\mathbb{V}_i} = \frac{1}{M_{\mathbb{V}_i}} \sum_{q \in \mathbb{V}_i} cf(q)^2 \frac{q}{||q-p_i||} \frac{dg(||q-p_i||)}{d||q-p_i||}, \tag{12}$$

where q is a sampled point inside the Voronoi region $\mathbb{V}_i$ corresponding to the ith sensor at the planar position p_i. Then we update the planar position of the ith sensor to $C_{\mathbb{V}_i}$.

As discussed in Sec. IV, *conformal factor (cf)* is used to compensate the metric distortion from $3D$ surface to $2D$ disk. cf of a vertex v_i can be computed as the ratio of the triangle areas in $3D$ and $2D$ spaces of all f_i^{jk} incident to v_i,

$$cf(v_i) = \frac{\sum_{f_i^{jk} \in F} Area_{3D}(f_i^{jk})}{\sum_{f_i^{jk} \in F} Area_{2D}(f_i^{jk})}.$$

cf of a point q within a triangle f_i^{jk} can be computed by bilinear interpolation,

$$cf(q) = \lambda_1 cf(v_i) + \lambda_2 cf(v_j) + \lambda_3 cf(v_k),$$

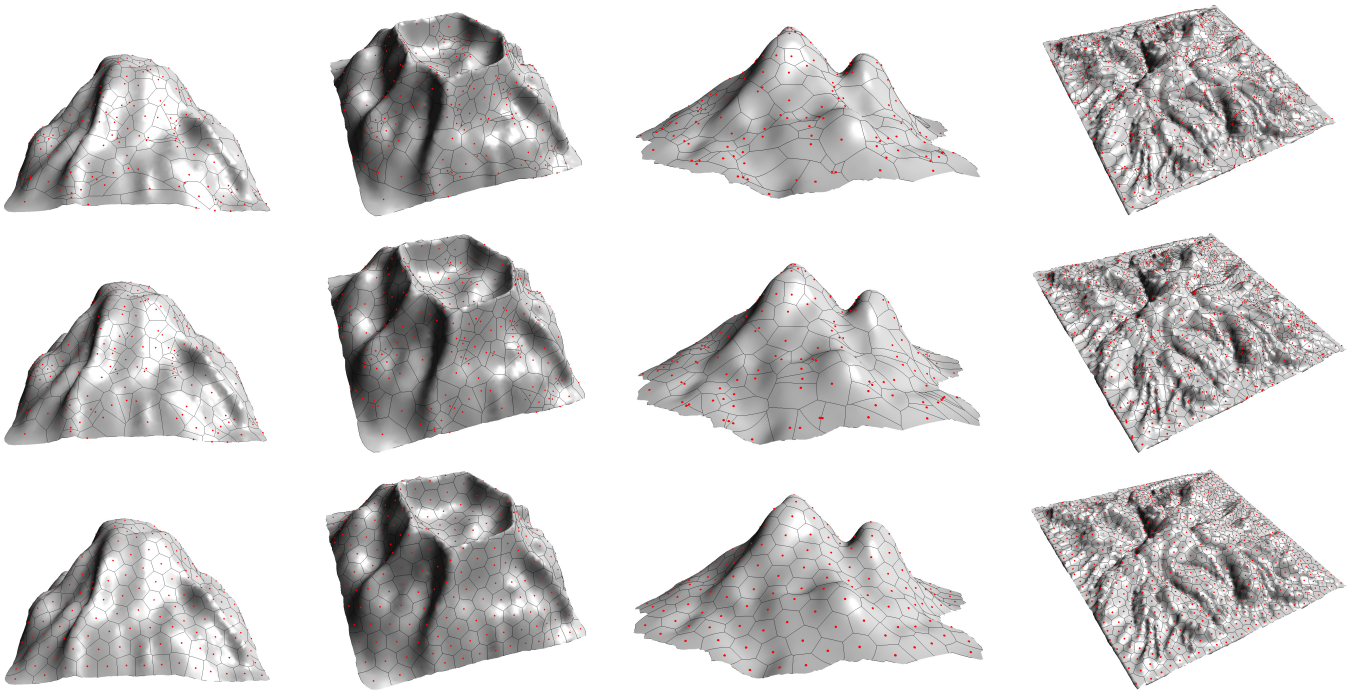

(a) Mountain 1 (b) Mountain 2 (c) Mountain 3 (d) Mountain 4

Fig. 2. Given a fixed set of sensors, the first row shows that the sensors are randomly deployed on surfaces with random sensing partition; the second row shows that the sensors are randomly deployed on surfaces with the Voronoi-based sensing partition; the third row shows that the sensors are re-deployed on surfaces with the generalized centroidal Voronoi based sensing partition. Figure 3 shows the decreased sensing unreliability of the networks.

where λ_1, λ_2, and λ_3 are barycentric coordinates of q inside f_i^{jk}, satisfying $\lambda_1+\lambda_2+\lambda_3 \equiv 1$.

VII. Performance Evaluation

We conduct simulations on various triangulated mountain surface models with complicated shapes and irregular boundaries. Specifically, mountain 1 model shown in Fig. 2(a) has the size of $720 \times 720m^2$, with the height $500m$, and approximated by $5k$ triangles. Mountain 2 model shown in Fig. 2(b) is a volcano with the size $720 \times 720m^2$ and the height $288m$, approximated by $10k$ triangles. Mountain 3 model shown in Fig. 2(c) has an irregular size of $900 \times 900m^2$, with the height $550m$, and approximated by $20k$ triangles. Mountain 4 model shown in Fig. 2(d) has the size of $1800 \times 1800m^2$, with the height $300m$, and approximated by $38k$ triangles.

A. Decreased Sensing Unreliability

Initially sensors are randomly deployed on the testing surface models, specifically, mountain 1 model with a given set of 300 sensors; mountain 2 model with a given set of 300 sensors; mountain 3 model with a given set of 200 sensors; mountain 4 model with a given set of 800 sensors. The first row of Fig. 2 shows that the sensors are randomly deployed on surfaces with a random sensing partition, which exhibits a very high sensing unreliability as given in Fig. 3. When the sensing area is re-partitioned based on Voronoi partition of the set of sensors, the sensing unreliability decreases 47.58% in average on the testing models. When we re-deploy those sensors such that they satisfy a generalized centroidal Voronoi partition on surface, the total sensing unreliability of a wireless sensor network decreases dramatically 89.94% in average compared with the random sensing deployment. Note that the sensing unreliability function is $g(||q-p_i||) = \frac{1}{2}||q-p_i||^2$. Fig. 3 experimentally shows the results of the Lemma 1 and the Theorem 1.

B. Unreliability Function

Theorem 1 is independent of the choice of the unreliability function. The sensing unreliability in our simulations given in Fig. 2 and 3 increases quadratically with the distance, with the unreliability function $g(||q-p_i||) = \frac{1}{2}||q-p_i||^2$. We also conduct simulations with other sensing unreliability functions. Given the same set of 300 sensors initially randomly deployed on mountain 1 model as shown in Fig. 2, two testings are conducted with the sensing unreliability increasing linearly and cubically, with $g(||q-p_i||) = ||q-p_i||$ and $g(||q-p_i||) = \frac{1}{3}||q-p_i||^3$ respectively. Fig. 5 shows the computed optimal positions of sensors and their sensing partitions. Fig. 4 gives the decreased sensing unreliability of the whole network.

C. Special Scenarios

In some special scenarios, the sensing reliability of a sensor under its sensing range does not have a noticeable decrease with the distance. Then the unreliability function can be defined as the following:

$$g(||q-p_i||) = \begin{cases} 1, & ||q-p_i|| \le R_s \\ \infty, & ||q-p_i|| > R_s, \end{cases}$$

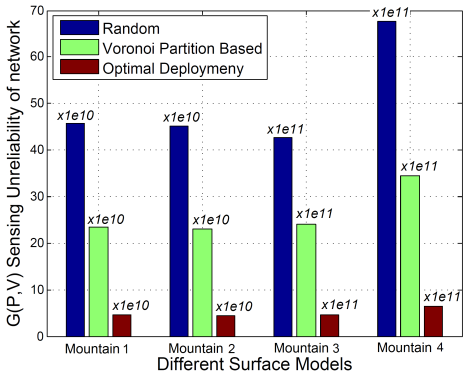

Fig. 3. Sensing unreliability with different deployment and sensing partition methods on various surface models shown in Figs. 2, where sensing unreliability function $g(||q-p_i||) = \frac{1}{2}||q-p_i||^2$.

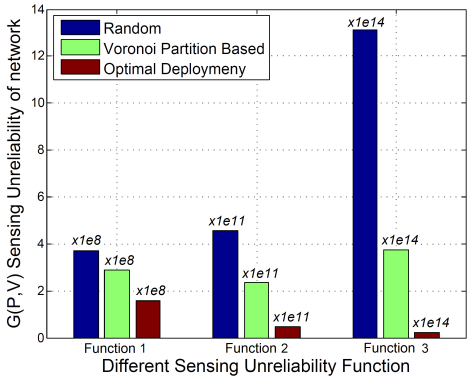

Fig. 4. Sensing unreliability of the same set of sensors deployed on mountain 1 surface with different deployment and sensing partition methods and various sensing unreliability functions, specifically, function 1 $g(||q-p_i||) = ||q-p_i||$, function 2 $g(||q-p_i||) = \frac{1}{2}||q-p_i||^2$, and function 3 $g(||q-p_i||) = \frac{1}{3}||q-p_i||^3$.

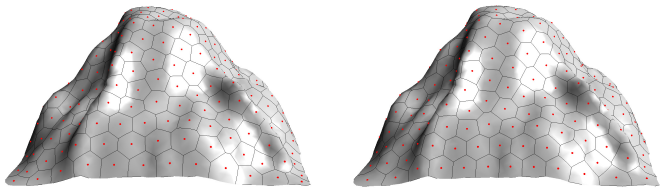

(a) $g(||q-p_i||) = ||q-p_i||$ (b) $g(||q-p_i||) = \frac{1}{3}||q-p_i||^3$

Fig. 5. The computed optimal positions of sensors and their sensing partitions on mountain 1 model with the same given set of sensors, but different sensing unreliability functions.

where R_s is a constant called sensing range. The accuracy of the collected data is guaranteed as long as it is acquired within the sensing range of the collecting sensor. A point q is said covered by a sensor if their distance is less than R_s. Under this special $g(||q-p_i||)$, a full covered sensor network, where every point on the surface is covered by at least one sensor, can obviously provide all the accurate data. To achieve the lowest unreliability in data acquisition, we are actually looking for a surface deployment scheme with full sensor coverage. The optimal surface deployment problem (OSDP) is then converted to the optimal surface coverage problem (OSCP) [27], the minimal number of sensors to fully cover the FoI on a surface. The hardness of the OSCP has been proved in [27]. There are several approximation algorithms proposed in [27] to address this problem in wireless sensor networks. With a slight change of our algorithms made by replacing Equation 12 to the following one:

$$C_{V_i} = \frac{\sum_{q\in V_i} cf(q)^2 q}{\sum_{q\in V_i} cf(q)^2} \tag{13}$$

when computing the centroid of each planar Voronoi region, our proposed algorithm in Sec. VI can also provide an approximated solution.

We choose the greedy method proposed in [27] to make a comparison because the greedy method performs the best in their simulations. We also compare with the triangle pattern [57], which is the most widely used method to cover FoI on an ideal plane, to illustrate the intrinsic limitation to directly apply planar deployment based method to surface. The sensing radius is 30m in our testings.

Fig.s 6 and 7 compare our method with the above two methods, where the partition of FoI on a surface for the greedy method is $D = 5$. Our approximation method achieves the highest coverage ratio under the same set of sensors for the same surface model. Note that Theorem 1 can no longer be applied here. But to maximize the coverage ratio of a given set of sensors on a FoI, it is a natural way to consider positioning sensors uniformly on a FoI to minimize the overlapping part of their sensing regions. The equation 13 is a discrete approximation of Equation 4, the computation of the mass centroid of a Voronoi region with constant mass density ($\rho(q) = 1$). So we actually compute a centroidal Voronoi partition of a given set of sensors with FoI on a $3D$ surface with constant density. Although it is Gershos conjecture [58] that the sites of an Euclidean centroidal Voronoi partition are uniformly distributed in the space for R^n and has been proved by Fejes Tóth only for 2D convex polygon case [59], extensive experiments have verified this conjecture [39], [40].

VIII. Discussions

This section includes discussions on time complexity of the proposed algorithm and the connectivity in sensor networks.

A. Time Complexity and Computation Time

Our proposed algorithm consists of two major steps: computing a conformal map and computing a generalized centroidal Voronoi partition. The tool to compute conformal map is discrete surface Ricci flow [60]. Its time complexity, which is dominated by the number of iterations, is given by $-C\frac{log\varepsilon}{\delta}$, where C is a constant, ε is the threshold of curvature error, and δ is the step length of each iteration [51]. Its convergence is guaranteed as proved in [51]. We measure the number of iterations required to get a successful planar mapping for mountain 1 model. Fig. 8 gives the result with $\varepsilon = 1e-4$ and $\delta = 1e-1$.

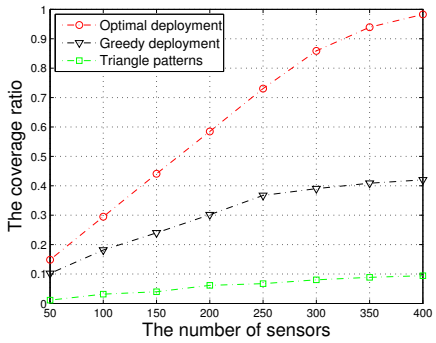

Fig. 6. Comparison of our proposed method with the greedy method and the triangle pattern on mountain 1 model.

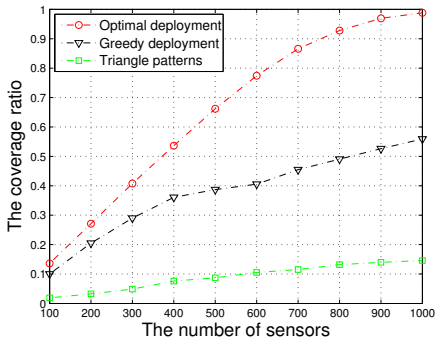

Fig. 7. Comparison of our proposed method with the greedy method and the triangle pattern on mountain 4 model.

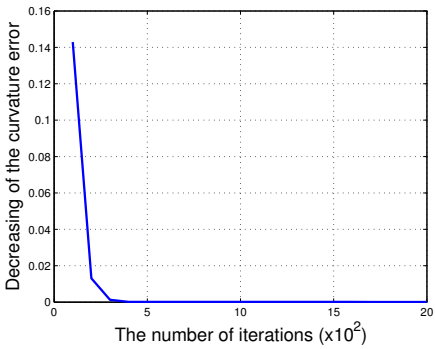

Fig. 8. The number of iterations required to meet a given curvature error threshold when computing a conformal map on mountain 1 model.

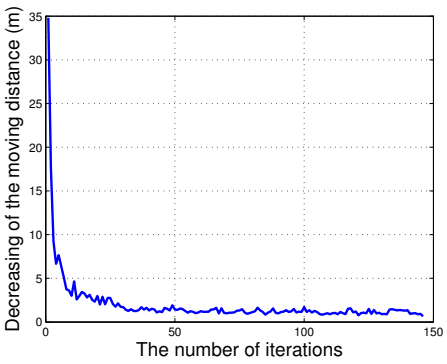

Fig. 9. The number of iterations required to meet a given moving distance threshold when computing a generalized centroidal Voronoi partition on mountain 1 model.

The time complexities of computing the Voronoi partition and the centroid are $O(n\log n)$ and $O(m)$ respectively, where n is the number of the sensors, and m is the number of the sampling points inside the unit planar disk for performing intergration. So the time complexity of one iteration of computing the generalized centroidal Voronoi partition is $O(n\log n+m)$. The total number of iterations depends on individual cases for convergence of the generalized centroidal Voronoi partition. Fig. 9 gives the number of iterations to compute a generalized centroidal Voronoi partition for mountain 1 model where the threshold of the maximum moving distance is $0.5m$. The average computing time of each iteration is 0.67 sec and the total computing time is 97.9 sec. Our testing computer has 1G memory with Intel Core2 X6800 3.0G Hz.

B. Connectivity of Sensor Network

In this research, we focus on sensing quality of a sensor network. Let r denote the longest distance between a sensor and a point inside its sensing region, and r_c denote the communication range of the sensor. If $\frac{r_c}{r} \geq 2$, a sensor node has a regular connectivity of six under our proposed deployment scheme when we assume numerical error free. The reason is that centroidal Voronoi partition in $\mathbb{R}^2$ always has congruent regular hexagons as its Voronoi regions [61], and the inverse of conformal mapping keeps the neighboring relations of each Voronoi region. For different degrees of connectivity of sensor networks deployed on surfaces, they remain open problems.

IX. Conclusion and Future Work

In this paper we have formulated the optimal surface deployment problem by introducing a general function to measure the sensing unreliability of the entire network on the FoI. We have proven that the optimal surface deployment can be achieved under a generalized centroidal Voronoi partition. Based on the insight gained from conformal mapping, we have proposed a series of algorithms to compute the optimal sensor deployment on 3D surfaces that minimizes the overall sensing unreliability of the network. The effectiveness of the proposed algorithms have been verified by simulation results.

Our current research considers static sensors that can be deployed at pre-determined locations. Our future work will take mobile sensors into consideration for hostile environment where sensors cannot be manually deployed. Besides the optimal sensing unreliability, different surface deployment optimization objectives will be studied in our future work.

Acknowledgements

M. Jin is partially supported by NSF CNS-1018306 and CCF-1054996. H. Wu is partially supported by NSF CNS-1018306. L. Shuai and X. Guo are partially supported by NSF CNS-1012975 and IIS-1149737.

References

[1] S. Meguerdichian, F. Koushanfar, M. Potkonjak, and M. B. Srivastava, "Coverage Problems in Wireless Ad-hoc Sensor Networks," in *Proc. of INFOCOM*, pp. 1380–1387, 2001.

[2] K. Kar and S. Banerjee, "Node Placement for Connected Coverage in Sensor Networks," in *Proc. of Ad Hoc and Wireless Networks and Workshops*, 2003.

[3] X.-Y. Li, P.-J. Wan, and O. Frieder, "Coverage in Wireless Ad Hoc Sensor Networks," *IEEE Transactions on Computers*, vol. 52, no. 6, pp. 753–763, 2003.

[4] X. Wang, G. Xing, Y. Zhang, C. Lu, R. Pless, and C. Gill, "Integrated Coverage and Connectivity Configuration in Wireless Sensor Networks," in *Proc. of SenSys*, pp. 28–39, 2003.

[5] B. Liu, P. Brass, O. Dousse, P. Nain, and D. Towsley, "Mobility Improves Coverage of Sensor Networks," in *Proc. of MobiHoc*, pp. 300–308, 2005.

[6] M. Cardei, M. Thai, Y. Li, and W. Wu, "Energy-Efficient Target Coverage in Wireless Sensor Networks," in *Proc. of INFOCOM*, pp. 1976–1984, 2005.

[7] S. Kumar, T. H. Lai, and A. Arora, "Barrier Coverage With Wireless Sensors," in *Proc. of MobiCom*, pp. 284–298, 2005.

[8] L. Lazos and R. Poovendran, "Stochastic Coverage in Heterogeneous Sensor Networks," *ACM Transactions Sensor Networks*, vol. 2, no. 3, pp. 325–358, 2006.

[9] A. Chen, S. Kumar, and T. H. Lai, "Designing Localized Algorithms for Barrier Coverage," in *Proc. of MobiCom*, pp. 63–74, 2007.

[10] P. Balister, B. Bollobas, A. Sarkar, and S. Kumar, "Reliable density estimates for coverage and connectivity in thin strips of finite length," in *Proc. of MobiCom*, pp. 75–86, 2007.

[11] W. Wang, V. Srinivasan, and K.-C. Chua, "Trade-Offs Between Mobility and Density for Coverage in Wireless Sensor Networks," in *Proc. of MobiCom*, pp. 39–50, 2007.

[12] X. Bai, D. Xuan, Z. Yun, T. H. Lai, and W. Jia, "Complete Optimal Deployment Patterns for Full-Coverage and k-Connectivity ($k \leq 6$) Wireless Sensor Networks," in *Proc. of MobiHoc*, pp. 401–410, 2008.

[13] Y. Bejerano, "Simple and Efficient K-Coverage Verification Without Location Information," in *Proc. of INFOCOM*, pp. 291–295, 2008.

[14] A. Saipulla, C. Westphal, B. Liu, and J. Wang, "Barrier coverage of line-based deployed wireless sensor networks," in *Proc. of INFOCOM*, pp. 127–135, IEEE, 2009.

[15] P. Balister, Z. Zheng, S. Kumar, and P. Sinha, "Trap coverage: Allowing coverage holes of bounded diameter in wireless sensor networks.," in *Proc. of INFOCOM*, pp. 136–144, IEEE, 2009.

[16] S. R. S. Sankararaman, A. Efrat and J. Taheri, "Scheduling sensors for guaranteed sparse coverage," in *Proc. of CoRR*, 2009.

[17] G. Yang and D. Qiao, "Multi-Round Sensor Deployment for Guaranteed Barrier Coverage," in *Proc. of INFOCOM*, 2010.

[18] X. Bai, Z. Yun, D. Xuan, W. Jia, and W. Zhao, "Pattern Mutation in Wireless Sensor Deployment," in *Proc. of INFOCOM*, pp. 1–9, 2010.

[19] N. Bartolini, T. Calamoneri, T. F. La Porta, and S. Silvestri, "Autonomous deployment of heterogeneous mobile sensors," *IEEE Transactions on Mobile Computing*, vol. 10, pp. 753–766, 2011.

[20] Z. Yu, J. Teng, X. Bai, D. Xuan, and W. Jia, "Connected coverage in wireless networks with directional antennas," in *Proc. of INFOCOM*, pp. 2264–2272, IEEE, 2011.

[21] C.-F. Huang, Y.-C. Tseng, and L.-C. Lo, "The Coverage Problem in Three-Dimensional Wireless Sensor Networks," in *Proc. of GLOBECOM*, pp. 3182–3186, 2004.

[22] M. K. Watfa and S. Commuri, "A Coverage Algorithm in 3D Wireless Sensor Networks," in *Proc. of the 1st International Symposium on Wireless Pervasive Computing*, pp. 10–16, 2006.

[23] S. M. N. Alam and Z. J. Haas, "Coverage and Connectivity in Three-Dimensional Networks," in *Proc. of MobiCom*, pp. 346–357, 2006.

[24] S. Oktug, A. Khalilov, and H. Tezcan, "3D Coverage Analysis under Heterogeneous Deployment Strategies in Wireless Sensor Networks," in *Proc. of the 2008 Fourth Advanced International Conference on Telecommunications*, pp. 199–204, 2008.

[25] T. Andersen and S. Tirthapura, "Wireless Sensor Deployment for 3D Coverage With Constraints," in *Proc. of The International Conference on Networked Sensing Systems*, pp. 78–81, 2009.

[26] C. Zhang, X. Bai, J. Teng, D. Xuan, and W. Jia, "Constructing Low-Connectivity and Full-Coverage Three Dimensional Sensor Networks," *IEEE Journal on Selected Areas in Communications (JSAC), Simple Wireless Sensor Networking Solutions*, 2010.

[27] M.-C. Zhao, J. Lei, M.-Y. Wu, Y. Liu, and W. Shu, "Surface Coverage in Wireless Sensor Networks," in *Proc. of INFOCOM*, pp. 109–117, 2009.

[28] X. Wang, G. Xing, Y. Zhang, C. Lu, R. Pless, and C. Gill, "Integrated coverage and connectivity configuration in wireless sensor networks," in *Proc. of SenSys*, pp. 28–39, 2003.

[29] Z. Zhou, S. Das, and H. Gupta, "Connected k-coverage problem in sensor networks," in *Proc. of ICCCN*, pp. 373–378, 2004.

[30] S. Yang, F. Dai, M. Cardei, J. Wu, and F. Patterson, "On connected multiple point coverage in wireless sensor networks," *Journal of Wireless Information Networks*, vol. 2006, 2006.

[31] G. Simon, M. Molnr, L. Gnczy, and B. Cousin, "Dependable k-coverage algorithms for sensor networks," in *Proc. of IMTC*, 2007.

[32] X. Bai, Z. Yun, D. Xuan, B. Chen, and W. Zhao, "Optimal multiple-coverage of sensor networks ," in *Proc. of INFOCOM*, pp. 2498–2506, 2011.

[33] Z. Butler and D. Rus, "Controlling mobile sensors for monitoring events with coverage constraints," in *Proc. of IEEE International Conference of Robotics and Automation*, pp. 1563–1573, 2004.

[34] J. Cortes, S. Martinez, T. Karatas, and F. Bullo, "Coverage control for mobile sensing networks," *IEEE Transactions on Robotics and Automation*, vol. 20, pp. 243–255, 2004.

[35] F. Bullo, J. Corts, F. Bullo, and J. Corts, "Adaptive and distributed coordination algorithms for mobile sensing networks," in *Lecture Notes in Control and Information Sciences*, vol. 309, pp. 43–62, 2005.

[36] M. Schwager, J. Mclurkin, and D. Rus, "Distributed Coverage Control with Sensory Feedback for Networked Robots," in *Proc. of Robotics: Science and Systems*, 2006.

[37] Q. Du, V. Faber, and M. Gunzburger, "Centroidal Voronoi tessellations: Applications and algorithms," *SIAM Review*, vol. 41, no. 4, pp. 637–676, 1999.

[38] A. Okabe, B. Boots, K. Sugihara, and S. N. Chiu, *Spatial tessellations: concepts and applications of Voronoi diagrams*. John Wiley & Sons, 2nd ed., 1999.

[39] P. Alliez, É. C. de Verdière, O. Devillers, and M. Isenburg, "Centroidal Voronoi diagrams for isotropic surface remeshing," *Graphical Models*, vol. 67, no. 3, pp. 204–231, 2005.

[40] Q. Du, M. Gunzburger, and L. Ju, "Advances in studies and applications of centroidal Voronoi tessellations," *Numerical Mathematics: Theory, Methods and Applications*, vol. 3, no. 2, pp. 119–142, 2010.

[41] G. Rong, Y. Liu, W. Wang, X. Yin, X. Gu, and X. Guo, "GPU-assisted computation of centroidal Voronoi tessellation," *IEEE Transactions on Visualization and Computer Graphics*, vol. 17, no. 3, pp. 345–356, 2011.

[42] S. P. Lloyd, "Least Squares Quantization in PCM," *IEEE Transactions on Information Theory*, vol. 28, no. 2, pp. 129–137, 1982.

[43] Q. Du, M. Emelianenko, and L. Ju, "Convergence of the Lloyd Algorithm for Computing Centroidal Voronoi Tessellations," *SIAM J. Numer. Anal.*, vol. 44, no. 1, pp. 102–119, 2006.

[44] M. S. Floater and K. Hormann, "Surface parameterization: a tutorial and survey," in *In Advances in Multiresolution for Geometric Modelling*, pp. 157–186, Springer, 2005.

[45] A. Sheffer, E. Praun, and K. Rose, "Mesh parameterization methods and their applications," *Foundations and Trends in Computer Graphics and Vision*, vol. 2, pp. 105–171, 2006.

[46] K. Hormann, B. Lévy, and A. Sheffer, "Mesh parameterization: Theory and practice," in *ACM SIGGRAPH Course Notes*, 2007.

[47] R. Remmert, *Classical topics in complex function theory*. Springer-Verlag, 1998.

[48] W. Kuhnel, *Differential Geometry: Curves - Surfaces - Manifolds*. American Mathematical Society, 2005.

[49] G. Rong, M. Jin, and X. Guo, "Hyperbolic centroidal voronoi tessellation," in *Proc. of ACM Symposium of Solid and Physical Modeling*, pp. 117–126, 2010.

[50] R. S. Hamilton, "Three manifolds with positive Ricci curvature," *Journal of Differential Geometry.*, vol. 17, pp. 255–306, 1982.

[51] B. Chow and F. Luo, "Combinatorial Ricci Flows on Surfaces," *Journal Differential Geometry*, vol. 63, no. 1, pp. 97–129, 2003.

[52] W. P. Thurston, *Geometry and Topology of Three-Manifolds*. Princeton lecture notes, 1976.

[53] Shuttle Radar Topography Mission (SRTM). http://www2.jpl.nasa.gov/srtm/.

[54] Light Detection And Ranging data (LIDAR). http://atlas.lsu.edu/lidar/.

[55] M. de Berg, O. Cheong, M. van Kreveld, and M. Overmars, *Computational geometry: algorithms and applications*. Springer, 2000.

[56] Computational Geometry Algorithms Library (CGAL). http://www.cgal.org.

[57] R. Kershner, "The number of circles covering a set," *American Journal of Mathematics*, 1939.

[58] A. Gersho, "Asymptotically optimal block quantization," *IEEE Transactions on Information Theory*, vol. 25, pp. 373–380, 1979.

[59] G. F. Tóth, "A stability criterion to the moment theorem," *Studia Scientiarum Mathematicarum Hungarica*, vol. 38, pp. 209–224, 2001.

[60] M. Jin, J. Kim, F. Luo, and X. Gu, "Discrete Surface Ricci Flow," *IEEE Transactions on Visualization and Computer Graphics*, vol. 14, no. 5, pp. 1030–1043, 2008.

[61] D. J. Newman, "The hexagon theorem," *IEEE Transactions on Information Theory*, vol. 28, no. 2, pp. 137–139, 1982.